*Work supported by the U. S. Atomic Energy Commission.

[1]P. L. Patterson, J. Chem. Phys. 48, 3625 (1968).
[2]E. E. Ferguson, F. C. Fehsenfeld, and A. L. Schmeltekopt, *Advances in Atomic and Molecular Physics*, edited by D. R. Bates and Immanuel Estermann (Academic, New York, 1969), Vol. 5, Chap. 1, p. 46.
[3]C. P. deVries and H. J. Oskam, Phys. Letters 29A, 299 (1969).
[4]J. P. Kaplafka, H. Merkelo, and L. Goldstein, Phys. Rev. Letters 21, 970 (1968).
[5]P. D. Goldan and L. Goldstein, Phys. Rev. A138, 39 (1965).
[6]H. Margenau, Phys. Rev. 69, 508 (1946).
[7]H. Hermansdorfer, *Plasma Diagnostics*, edited by W. Lochte-Holtgreven (North-Holland, Amsterdam, 1968), Chap. 8, p. 478.
[8]L. Goldstein, in *Advances in Electronics and Electron Physics*, edited by L. Marton (Academic, New York, 1955), Vol. 7.
[9]J. M. Anderson and L. Goldstein, Technical Report No. 7, AFCRC Contract No. AF19(604)-524, Electrical Engineering Research Laboratory, University of Illinois, 1955 (unpublished).
[10]P. Molmud, Phys. Rev. 114, 29 (1959).
[11]H. S. W. Massey and E. H. S. Burhop, *Electronic and Ionic Impact Phenomena* (Oxford U. P., Oxford, England 1969), Vol. 1, Chap. 2, p. 83.
[12]Lothar Frommhold, Manfred A. Biondi, and F. J. Mehr, Phys. Rev. 165, 161 (1968).
[13]A. V. Phelps and J. P. Molnar, Phys. Rev. 89, 1202 (1953).
[14]W. A. Fitzsimmons, N. F. Lane, and G. K. Walters, Phys. Rev. 174, 193 (1968).
[15]Paul L. Patterson, Joint Institute for Laboratory Astrophysics, Report No. 87, University of Colorado, 1966 (unpublished).
[16]E. C. Beaty and P. L. Patterson, Phys. Rev. A137, 346 (1965).
[17]D. R. Bates, A. E. Kingston, and R. W. P. McWhirter, Proc. Roy. Soc. (London) 267, 297 (1962).
[18]Jacques Berlande, Michel Cheret, Robert Deloche, Alain Gonfalone, and Claude Manus, Phys. Rev. A 1, 887 (1970).
[19]A. V. Phelps (private communication).
[20]J. C. Ingraham and Sanborn C. Brown, Phys. Rev. A138, 1015 (1965).
[21]A. V. Phelps, O. T. Fundingsland, and Sanborn C. Brown, Phys. Rev. 84, 559 (1951).
[22]Edward C. Jordan, *Electromagnetic Waves and Radiating System* (Prentice-Hall, Englewood Cliffs, N. J., 1950), Chap. 9.

PHYSICAL REVIEW A VOLUME 3, NUMBER 1 JANUARY 1971

Inelastic Scattering of Electrons and Protons by the Elements He to Na†

Eugene J. McGuire
Sandia Laboratories, Albuquerque, New Mexico 87115
(Received 16 July 1970)

We have calculated discrete and continuum generalized oscillator strengths for all the occupied shells of He–Na and the 3*s* and 3*p* continuum generalized oscillator strengths for Ar. The calculations are done with a one-electron common-central-potential unrelaxed-core approximation. The generalized oscillator strengths were used to compute proton-excitation and -ionization cross sections and stopping power, electron-ionization cross sections, and neutral-neutral-ionization and -stripping cross sections. For proton ionization above 200 keV and electron ionization above 200 eV, the calculated cross sections are in better than 20% agreement with experiment. The calculated proton stopping power is lower than experiment by 25% at 100 keV and within 10% at 1 MeV. The computed He-He ionization cross section agrees with the measurement by Wittkower, Levy, and Gilbody, while the computed He-Ar ionization cross section is a factor of 5 higher than the measurement by Puckett, Taylor, and Martin.

I. INTRODUCTION

The generalized oscillator strength was introduced by Bethe[1] and used in his stopping-power theory.[1,2] Bethe's stopping-power formula uses the optical oscillator strength, and for many years the generalized oscillator strength remained unexplored. Lassettre's[3] electron scattering experiments provided the first extensive experimental measurements of atomic and molecular generalized oscillator strengths. These experimental generalized-oscillator-strength measurements have been applied by Green and Peek[4] to certain molecular scattering problems. Rau and Fano[5] have obtained asymptotic properties of generalized oscillator strengths. Inokuti and Kim[6] and Oldham[7] have done accurate calculations of generalized oscillator strengths for a limited number of discrete excitations in He. Bell, Kingston, and Kennedy[8] have done similar calculations for a wider range of discrete excitations with a less accurate ground-state wave function. Bell and Kingston[9] have done proton and electron ionization for He, and Oldham[10] has done proton ionization for He.

Our purpose is to use the generalized-oscillator-strength (GOS) approach in calculations for a wide

range of elements to ascertain where the Born approximation with approximate one-electron wave functions will lead to results in reasonable agreement with experiment. The one-electron model we use is crude relative to the accurate He calculations[6-10] for the ground and excited discrete states. This is reflected in the excitation-cross-section calculations. However, the He electron and proton-ionization cross-section calculations are in excellent agreement with the more accurate calculations. Peach[11] has done calculations for proton and electron ionization in the elements He–Ar. The continuum one-electron orbital used was, in general, a hydrogenic one. In general, Peach's calculations are higher than experiment by a factor of 2 at large proton and electron energies. We will show this factor of 2 in Peach's calculations can be reduced by using a more accurate continuum orbital.

These calculations are based on an exactly solvable one-electron common-central-field unrelaxed-core model wherein we approximate the quantity $[-rV(r)]$ of Herman and Skillman[12] by a series of straight lines. With this model we have made extensive calculations of atomic photo-ionization cross sections.[13] For the light elements (He–Na), the calculated photo-ionization cross sections agree with experiment to 10% (except for some elements near threshold), indicating that the calculated optical-oscillator-strength function (the zero-momentum transfer limit of the GOS) is accurate. With this in mind we have computed the GOS for the filled shells of He–Na. The calculated $3p$ photo-ionization cross section of Ar [13,14] differs significantly from the measured cross section; the calculated cross section is too high at threshold and drops off more rapidly with increasing photon energy than does the measurement. This difference persists in the ionization cross section for the $4p$ shell of Kr and the $5p$ shell of Xe. To examine the effect of this on electron- and proton-ionization cross sections, we have computed the GOS for the $3s$ and $3p$ shells of Ar.

In Sec. II we discuss the calculation of the GOS and compare our model calculations with other calculations and some experimental data. All the calculated values are available from the author.[15] In Sec. III we report the electron- and proton-ionization cross section and proton-stopping-power calculations, and in Sec. IV discuss the neutral-neutral calculations.

II. CALCULATION OF GENERALIZED OSCILLATOR STRENGTHS

A. Calculational Procedures

As mentioned in the Introduction, we approximate the quantity $[-rV(r)]$ of Herman and Skillman by a series of straight lines. For He–Na we use four straight lines and for Ar, five. To check the dependence of the computed GOS on the number of straight lines, we recomputed the Ne $2p$ continuum GOS using five straight lines. The maximum difference between the two sets of GOS was 5%. The difference in cross section and stopping power was less than 1% with the two sets of GOS. This is one specific case, and while we consider it typical, there is no guarantee that the model used will not introduce errors larger than the above in other continuum GOS. As in the photo-ionization calculations[13] there are a number of approximations in the computed GOS matrix elements. We use a one-electron model, with a common central field; we also use the unrelaxed-core approximation. As a result of these approximations the one-electron orbitals in the product wave functions for the initial and final states reduce the GOS matrix element to a simple one-electron matrix element. The GOS per nl electron per $\epsilon l'$ (continuum) hole is then

$$\frac{df_{nl}}{d\epsilon}(\epsilon,\ K^2,\ l') = \Delta E/K^2 \left| \langle nl \left| e^{i\vec{K}\cdot\vec{r}} \right| \epsilon l' \rangle \right|^2, \quad (1)$$

where $\Delta E = \epsilon - E_{nl}$ is in rydbergs (13.6 eV), $-E_{nl}$ is the one-electron ionization energy of the nl shell, ϵ is the continuum energy with $\epsilon = 0$ at the ionization threshold, r is in Bohr radii and K in inverse Bohr radii, with $df/d\epsilon$ in Ry^{-1}. Expanding the exponential in Eq. (1) in Legendre polynomials and Bessel functions leads to

$$\frac{K^2}{\Delta E}\frac{df_{n0}}{d\epsilon} = (2l'+1)\left| \int_0^\infty \left(\frac{\pi}{2Kr}\right)^{1/2} \times J_{l'+1/2}(Kr)\,\phi_{n0}(r)\phi_{\epsilon l'}(r)\,dr \right|^2, \quad (2)$$

$$\frac{K^2}{\Delta E}\frac{df_{nl}}{d\epsilon} = l'\left| \int_0^\infty \left(\frac{\pi}{2Kr}\right)^{1/2} J_{l'-1/2}(Kr)\,\phi_{nl}(r)\,\phi_{\epsilon l'}(r)\,dr \right|^2 + (l'+1)\left| \int_0^\infty \left(\frac{\pi}{2Kr}\right)^{1/2} J_{l'+3/2}(Kr) \times \phi_{nl}(r)\phi_{\epsilon l'}(r)\,dr \right|^2 .$$

The orbitals ϕ, with their asymptotic properties and generating scheme, are defined in Ref. 13.

Our computed continuum GOS is a section of the true GOS; that is, the computations extend over the range $0 \le \epsilon \le \epsilon_c$, $0 \le K^2 \le K_c^2$, and $0 \le l' \le l'_c$, where ϵ_c, K_c^2, and l'_c are cutoff values. K_c^2 was taken to be sufficiently large that for fixed ϵ all significant structure in the GOS occurred for $k^2 < K_c^2$, and such that for $K^2 > K_c^2$ the GOS would be approximated by $f(K^2, \epsilon) = A/K^{2\lambda}$. $|\lambda|$ was, in general, close to but smaller than the $|\lambda|$ determined by Rau and Fano.[5] To determine ϵ_c we use the expression for the proton-ionization cross section

$$\sigma = \frac{4\pi a^2}{(M_e/M_p)E_0} \int_0^{\epsilon_{max}} \frac{d\epsilon}{(\epsilon + E_I)} \times \int_{K^2_{min}}^{K^2_{max}} \sum_{l'=0}^{\infty} \frac{df_{nl}}{d\epsilon}(\epsilon, K^2, l') \frac{dK^2}{K^2} , \quad (3)$$

where E_0 is the incident proton energy (in Ry), a_0 is the Bohr radius, M_e amd M_p are the electron and proton masses, respectively. $E_I = |E_{nl}|$, the ionization energy, ϵ_{max} is the maximum energy of the secondary electron, and K^2_{max} is the maximum proton momentum transfer. K^2_{min} for incident protons is given by[1] $K^2_{min} = M_p(\Delta E)^2/2\hbar^2 E_0$, with K^2_{min} as well as ϵ_{max} and K^2_{max} arising from the kinematics. In addition we use the well-known[16,17] property of the GOS, that at large ϵ it is dominated by the Bethe ridge, so that the GOS is large only near $\epsilon/R = K^2 a_0^2$, where $R = 13.6$ eV. For the K^2 integral in Eq. (3) to produce a significant contribution at large ϵ one must have $K^2_{min} < \epsilon/Ra_0^2 = 2M_e\epsilon/\hbar$, or for $\epsilon \gg E_I$, $\epsilon < 4M_eE_0/M_p$. Our calculations are limited to $E_0 \leq 1$ MeV, which leads to $\epsilon < 160$ Ry. For all these calculations we chose $\epsilon_c = 200$ Ry. This is illustrated in Fig. 1, where the solid lines labeled E indicate the region

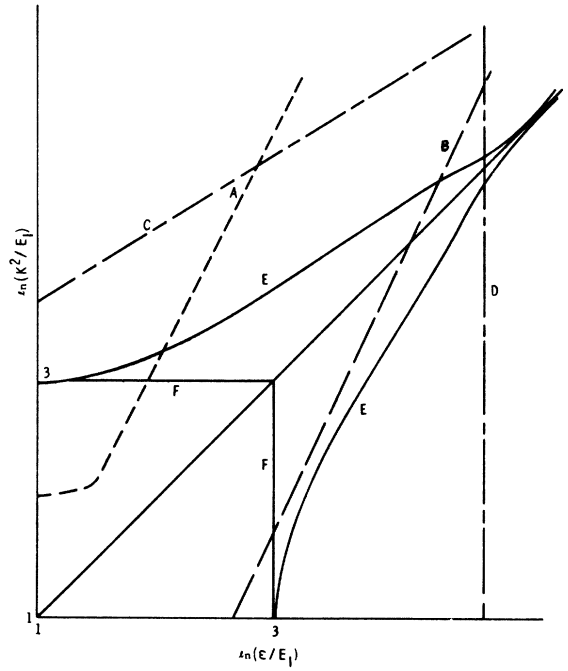

FIG. 1. Sketch of region of ϵ, K^2 plane significant to these GOS calculations. Curves labeled E bound the region of the plane where the GOS is significant, while the square labeled F bounds the region wherein subshell GOS shows individual structure. Curves A and B are K^2_{min} for low and high incident proton energies, respectively, and when B corresponds to 1-MeV proton energy, lines C and D bound the region in which the GOS was computed.

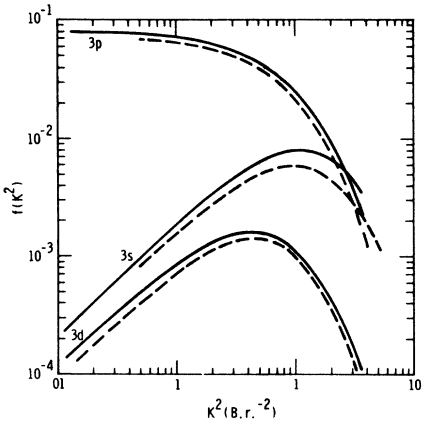

FIG. 2. Helium 1s-3s, 3p, 3d generalized oscillator strengths. Solid curves are our calculations; dashed 1s-3s, 3p curves are from Ref. 6 and dashed 1s-3d from Ref. 8.

in the $\ln(K^2/E_I)\ln(K^2/E_I)$, $\ln(\epsilon/E_I)$plane, where the GOS is significant. The solid square labeled F indicates the region where distincitive features of particular subshell GOS appear (discussed in Sec. II B). The dashed curves A and B represent K^2_{min} for small and large E_0, respectively. If the dashed curve B corresponds to $E_0 = 1$ MeV, then the broken curves D and C represent $\ln(\epsilon_c/E_I)$ and $\ln(K_c^2(\epsilon)/E_I)$, indicating the region over which we compute the GOS.

Since we do not use hydrogenic orbitals, we cannot do the sum over l' in Eq. (3) in closed form. In the region of the Bethe ridge one finds that many l' continuum orbitals contribute significantly to the GOS. Arguing that a ground-state orbital of ionization energy E_I(Ry) has its outermost peak at $r = 1/\sqrt{E_I}$, and that only those orbitals whose turning points occur at smaller radii contribute to the GOS, leads to the criterion that those orbitals must be included for which

$$l'(l'+1) < \epsilon/E_I , \quad (4)$$

where the energies are in Ry. For ionization of complete shells where $E_I > 1.2$ Ry and $\epsilon = 200$ Ry, a maximum l' of 13 is sufficient. Because of computer time limitations we stopped at $l'_c = 11$, for 25 Ry $\leq \epsilon \leq$ 200 Ry. For $0 \leq \epsilon \leq 1$ Ry we stopped at $l' = 4$, and for 1 Ry $< \epsilon <$ 25 Ry we stopped at $l' = 6$. The expression for stopping power due to ionization is obtained by dropping the $(\epsilon + E_I)$ denominator in Eqs. (3). The effect of dropping terms in the l' sum is significant for the stopping-power calculation but not in the ionization cross-section calculation. For both Na 3s ($E_I = 0.378$ Ry) and Ne 2p ($E_I = 1.47$ Ry), for which the above criterion indicates $l_c = 23$ and $l_c = 12$, respectively, should apply, we performed the ionization cross-section and stopping-power calculations with $l_c = 6$ and $l_c = 11$. At 1 MeV proton

energy there was less than 1% difference in the calculated ionization cross section in the two cases for both elements. However, with $l_c = 11$ the contribution of ionization to the stopping power was 5% higher for Ne $2p$ and 20% higher for Na $3s$ than with $l_c = 6$. But for Na at 1 MeV, ionization of the $3s$ shell contributes less than 7% to the total computed stopping power.

In addition to determining an asymptotic expression in K^2 for use in Eq. (3), we use the values of $d\sigma/d\epsilon$ at 150 and 200 Ry to determine an asymptotic expression in ϵ for $d\sigma/d\epsilon$. Between incident proton energies of 10 keV and 1 MeV the contribution of the asymptotic regions to the total cross section and stopping power was less than 10^{-3} of the total.

Finally we introduce a device to extend our direct calculations to higher incident proton energies. We argue that the Bethe ridge can be approximated by a δ function, so that

$$\frac{df_{nl}}{d\epsilon}(\epsilon, K^2) = \frac{df^0_{nl}}{d\epsilon}(\epsilon, K^2), \quad \frac{\epsilon}{R} < \frac{E_B}{R}, \quad K^2 a_0^2 < \infty$$

$$= \frac{Z}{R}\,\delta\left(\frac{\epsilon}{R} - K^2 a_0^2\right), \quad \frac{\epsilon}{R} \geq \frac{E_B}{R},\ K^2 a_0^2 \geq \frac{E_B}{R}\,. \tag{5}$$

In the other sector we have $df_{nl}(\epsilon, K^2) = 0$. E_B is an energy above which the GOS is dominated by the Bethe ridge. Z is in general a function of K^2 of the form[1]

$$Z = Z_{nl}\left[1 - \sum_{n'l'} f_{nl,n'l'}(K^2)\right],$$

where $fnl, n'l'$ is the oscillator strength for transitions to states forbidden by the Pauli exclusion principle, and Z_{nl} is the number of electrons in the nl subshell. Since we are using Z for the Bethe ridge region only, we can use $Z = Z_{nl}$. An examination of discrete excitation GOS indicates that the peak GOS falls off with increasing $E_{n'l'}$ and that for particular $E_{n'l'}$ the GOS falls off rapidly when $K^2 > E_{n'l'}$. Thus when $E_{n'l'} < E_B$ we can neglect $f_{nl,n'l'}$ because it is falling rapidly at those K^2 appropriate to the Bethe ridge, and for $E_{n'l'} > E_B$ because the peak GOS is small ($< 10^{-3}$).

Using Eq. (5) one can write expressions for the cross-section differential in secondary electron energy $d\sigma/d\epsilon$, and the ionization cross section and stopping power due to ionization for a specific subshell:

$$\frac{d\sigma}{d\epsilon}(E_0)\bigg|_{nl} = \frac{4\pi a_0^2 M_p}{M_e E_0(\epsilon + E_I)}\Bigg]\theta(E_B - \epsilon) \times \int_{K^2_{\min}}^{K^2_{\max}} \frac{df^0_{nl}(\epsilon, K^2)}{d\epsilon}\frac{dK^2}{K^2}$$

$$+ \frac{Znl}{\epsilon}\theta(\epsilon - E_B)\,\theta\left(\frac{4M_e}{M_p}E_0 - \epsilon\right)\Bigg]\,, \tag{6}$$

$$\sigma\Big|_{nl} = \frac{4\pi a_0^2 M_p}{M_e E_0}\left[\int_0^{E_B}\frac{d\epsilon}{(\epsilon + E_I)}\int_{K^2_{\min}}^{K^2_{\max}}\frac{df^0_{nl}}{d\epsilon}\frac{dK^2}{K^2}\right.$$

$$\left. + Z_{nl}\,\theta\left(\frac{4M_e}{M_p}E_0 - E_B\right)\left(\frac{1}{E_B} - \frac{M_p}{4M_e E_0}\right)\right]\,, \tag{7}$$

$$\frac{-1}{n}\frac{dE}{dx}\bigg|_{nl} = \frac{4\pi a_0^2 M_p}{M_e E_0}\left[\int_0^{E_B} d\epsilon \int_{K^2_{\min}}^{K^2_{\max}}\frac{df^0_{nl}}{d\epsilon}\frac{dK^2}{K^2}\right.$$

$$\left. + Z_{nl}\,\theta\left(\frac{4M_e}{M_p}E_0 - E_B\right)\ln\left(\frac{4M_e E_0}{M_p E_B}\right)\right]\,, \tag{8}$$

where θ is a step function.

With GOS determined up to $E_B = 200$ Ry, these expressions allow one to compute the relevant quantities for incident proton energies greater than 1 MeV. In Sec. III we make use of Eq. (8) in determining the stopping power of He for $E_0 > 1$ MeV.

B. The Computed GOS

As mentioned earlier the detailed GOS calculations are available.[15] Here we briefly discuss some features. Roughly speaking, and neglecting absolute magnitudes, the GOS for the nl shell as a function of scaled variables ϵ/E_{nl} and K^2/E_{nl} is independent of nuclear Z. Thus, the GOS for He $1s$, Be $2s$, Ne $2p$, Na $3s$, and Ar $3p$ ionization are similar to the GOS for the same shells in different atoms. In Fig. 1 we sketch the region in the $\ln(K^2/E_I)$, $\ln(\epsilon/E_I)$ plane where the GOS is not negligible. The solid square encloses the region where distinctive features for the different shells appear. Outside the square the Bethe ridge is

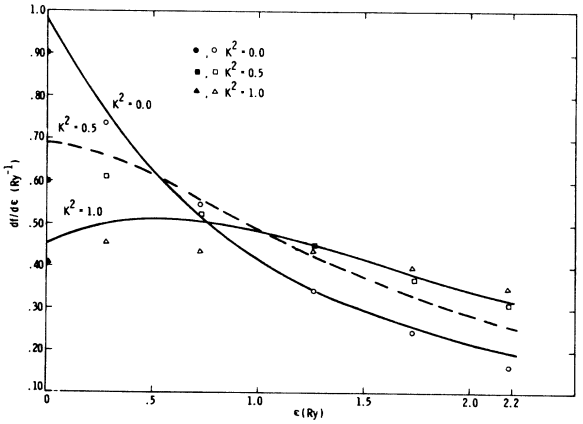

FIG. 3. He continuum generalized oscillator strengths as a function of ϵ for $K^2 = 0.0$, 0.5, and 1.0. Experimental values are from Ref. 3.

dominant. In the region of the Bethe ridge the GOS at $K^2 = 0$ drops off rapidly with increasing ϵ. For ϵ fixed the GOS is roughly constant for increasing K^2 until $K^2 \approx \frac{1}{3}\epsilon$, at which point the GOS increases until at $K^2 \approx \epsilon$ it is three orders of magnitude larger than at $K^2 = 0$. For $K^2 > \epsilon$ the GOS drops off rapidly. In the region enclosed by the square for both He 1*s* and Ne 2*p*, the GOS for small ϵ is a maximum at $K^2 = 0$. As we increase ϵ, the maximum shifts from $K^2 = 0$ to larger K^2, with the maximum at $K^2 < \epsilon$ until the Bethe ridge is reached. There is no indication of a zero in the GOS. For Be 2*s* there is no indication of a zero in the GOS, but for small ϵ the peak in the GOS appears at nonzero K^2, and as ϵ is increased the peak moves out in K^2 as in He 1*s* and Ne 2*p*. For both Na 3*s* and Ar 3*p* there is a zero in the optically allowed partial-wave GOS at $K^2 = 0$. This is seen in the photo-ionization cross section and arises from a zero in the $3s$-ϵp matrix elements for Na and a zero in the $3p$-ϵd matrix element coupled with a small magnitude for the $3p$-ϵs matrix element for Ar. The cause of this for $K^2 = 0$ is discussed in Ref. 14. The location of the zero in the partial GOS moves to increasing ϵ as K^2 is increased, but appears only in the optically allowed angular momentum partial GOS. With increasing K^2 the optically forbidden partial waves contribute to the total GOS washing out the effect of the zero.

In Fig. 2 we compare our calculated He $1s$-$3l'$ discrete excitation GOS with the calculations of Kim and Inokuti[6] for $1s$-$3s$ and $1s$-$3p$ and Bell *et al.*[8] for $1s$-$3d$. For the $1s$-$3p$ transition our result is 15% higher than the more accurate calculation, for $1s$-$3d$ the difference is 25%, and for $1s$-$3s$ it is 25% for $K^2 < 1$ and as much as a factor of two for large K^2. In Fig. 3 we compare our calculations with the measurements of Lassettre *et al.* for the limited experimental range studied. The calculations agree with experiment to 15%. However, the comparison shows a characteristic discrepancy that is present in all our computed GOS; the calculations are higher than experiment

TABLE I. Comparison of $f_{3s,\,nl}(0)$ and $df_{3s,\,nl}/dK^2 \mid K^2 = 0$ for Na. HR and opt. results are from Ref. 18.

Final state	f[a]	f_1[a]	f(calc)	f_1(calc)	f[a]
4*s*		3.5		1.4	
5*s*		0.58		0.20	
6*s*		0.11		0.074	
3*p*			0.970		0.975
4*p*	0.019		0.0146		0.014
5*p*	0.0021		0.00236		0.0021
3*d*		9.0		2.8	
4*d*		2.0		0.50	

[a]Results from Ref. 18.

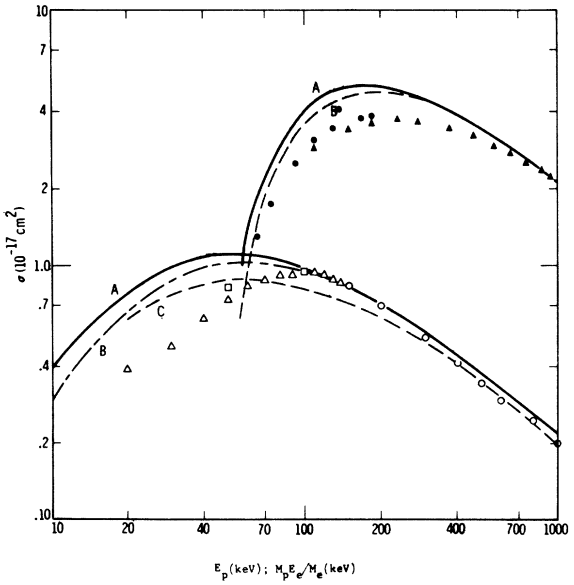

FIG. 4. Calculated He proton- and electron- (×10) ionization cross sections. Curves A are our calculations, curves B are from Ref. 9, and curve C from Ref. 19. Open triangles, squares, and circles are from Refs. 20, 24, and 21, respectively; solid circles and triangles from Refs. 22 and 23, respectively.

near $\epsilon = 0$ and lower than experiment at large ϵ. Effectively, the one-electron model squeezes the GOS in toward smaller ϵ. In Table I we compare our calculated Na $3s$-nl GOS with the electron-scattering measurements of Hertel and Ross[18] near $K^2 = 0.0$. Since the optical oscillator strength vanishes for $3s$-ns and $3s$-nd transitions, we compare the slopes f_1, where $f_1 = \lim df_{nl,n'l'}(K^2)/dK^2$ as $K^2 \to 0$. In addition we include the results of optical measurements. Clearly, for allowed transitions the calculations are in excellent (10%) agreement with the optical measurements, and in good agreement with the electron-impact measurements. However, for the forbidden transitions the calculated f_1 values are below experiment by a factor of 2.5 for the $3s$-ns transitions and a factor of 4 for the $3s$-nd transitions.

Finally, we used the optical limit to compute the mean excitation energy I that appears in the Bethe stopping-power formula[1,2]:

$$\ln I = \sum_{\substack{\text{occupied}\\ nl}} N_{nl} \sum_{\substack{n'l'\\ n'l' \neq nl}} N'_{n'l'} f_{nl,n'l'}(K^2 = 0.0) \times \ln(E_{n'l'} - E_{nl}) \Big/ \sum_{\substack{\text{occupied}\\ nl}} N_{nl} \sum_{\substack{n'l'\\ n'l' \neq nl}} N'_{n'l'} f_{nl,n'l'} \times (K^2 = 0.0)\,, \tag{9}$$

where the summation over $n'l'$ includes integration over the continuum, N_{nl} is the number of electrons in the nl shell, and $N'_{n'l'}$ is the number of holes in the $n'l'$ shell. In graphically integrating the continuum part of the numerator and denominator in Eq. (9) we estimate an error of 2–3% may occur. Since $\ln I \sim 2$ for I in rydbergs and $Z \geq 6$, the error in $I/Z \sim 5\%$ for $Z \geq 6$. In Table II we compare the calculated values of I/Z (in eV per nuclear charge) with the best experimental estimates.[17] Noteworthy is the variation of I/Z with Z. This is due to the large oscillator strength and small energy difference in $2s$-$2p$ and $3s$-$3p$ resonance transitions. Further, the calculated I/Z values are less than or equal to the best experimental estimates. This is an expected feature of calculated GOS which are squeezed in relative to the true values. However, in the Bethe stopping-power formula $-(1/n)dE/dx \propto \ln(4M_e E_0/M_p I)$. Thus an underestimate of I leads to an overestimate of $-(1/n)dE/dx$, while a direct calculation of $-(1/n)dE/dx$ using a squeezed GOS leads to an underestimate.

III. ELECTRON- AND PROTON-IONIZATION CROSS SECTIONS AND PROTON STOPPING POWER

The procedure used in determining cross sections and stopping power is to use Eq. (6) to find $d\sigma/d\epsilon$, and then integrate over ϵ to find σ and $-(1/n)dE/dx$. In Fig. 1 the curves labeled A and B are lower limits as a function of ϵ in the K^2 integration. Curve A is appropriate to large $K^2_{\min}$ or small E_0, and the integral over K^2 does not include either the small K^2 (optical) region nor the Bethe ridge. Curve B for higher E_0 and smaller $K^2_{\min}$ includes both the optical and Betheridge regions. For incident proton energies corresponding to curve A, one does not expect the Bethe stopping-power formula to be valid. However, we shall see in the He stopping-power results that the direct Born calculation of stopping power with these one-electron wave functions is also incorrect, because the GOS calculations in the region above curve A is poor.

For electron ionization the limits on the integrals in Eq. (3) were taken to be[1,11]

$$\epsilon_{\max} = \frac{E_0}{2}, \quad \left\{ \begin{matrix} K^2_{\max} \\ K^2_{\min} \end{matrix} \right\} = 2E_0 - \Delta E \pm 2[E_0(E_0 - \Delta E)]^{1/2} .$$

Our calculated proton stopping power includes only stopping power due to single excitation and single ionization. The excitation cross sections are not reported here but are available from the author. The results reported here emphasize He because extensive measurements and other calculations exist for He and because the discrepancies that appear between calculation and experiment for He, appear no worse than for the other elements.

In Fig. 4, we show the calculated proton- and

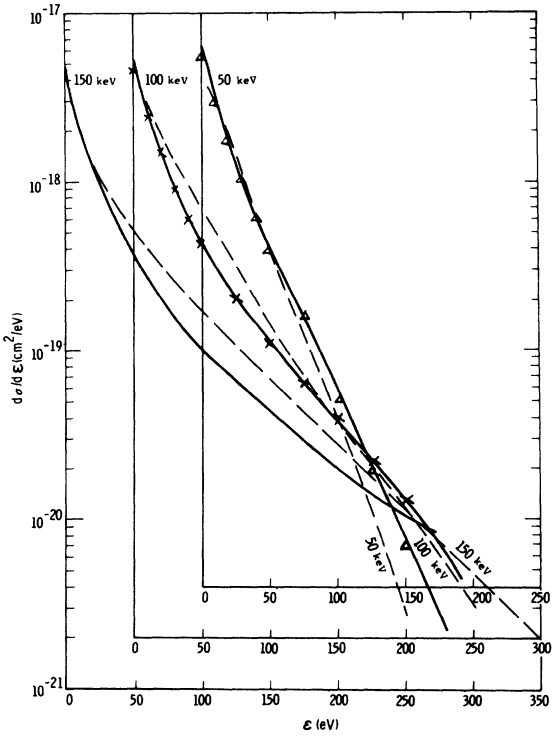

FIG. 5. Proton-ionization cross section of He as a function of secondary-electron energy. The format as well as dashed lines are taken from Ref. 24, and solid lines are the calculations. Triangles and crosses are from Ref. 9 for 50 and 100 keV, respectively.

electron-ionization cross sections of He, the calculations of Bell and Kingston,[9] and Mapleton,[19] and the proton measurements of deHeer *et al.*,[20] Hooper *et al.*,[21] and the electron measurements of Asundi and Kurepa,[22] and Rapp and Englander-Golden.[23] For clarity the electron-ionization results have been multiplied by 10, and plotted as a function of $M_p E_e/M_e$, where E_e is the incident electron energy. For proton energy greater than 150 keV and incident electron energy greater than 150 eV our calculations are in essential agreement with those of Bell and Kingston.[9] However, in Fig. 5, where we compare the calculated $d\sigma/d\epsilon$ with the measurements of Rudd and Jorgensen[24] (we plot the results in the format of Ref. 24), it can be seen that over a wide range of ϵ there is a significant disagreement. Yet our calculations are in excellent agreement with those of Bell and Kingston.[9] The effect of this disagreement is not apparent in the total ionization cross section, which is dominated by the small ϵ region of $d\sigma/d\epsilon$, but is clearly seen in stopping power. In Fig. 6 we show the stopping-power results for protons on He. The circles are stopping power due to ionization as computed by Rudd and Jorgensen from their $d\sigma/d\epsilon$ measurements. Dashed curve A is the computed ionization stopping

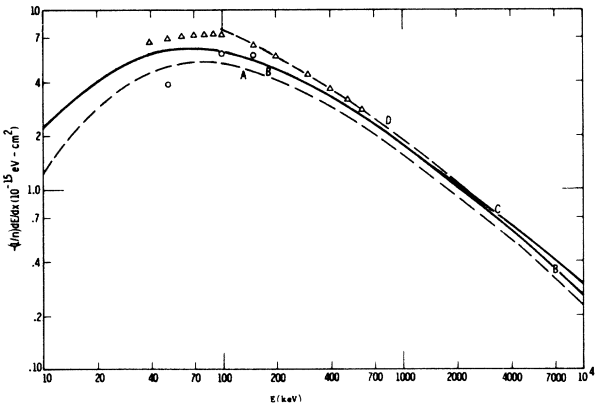

FIG. 6. Stopping power of He for protons. Curve A is the calculated stopping power due to ionization of electrons with up to 300 Ry of kinetic energy. Curve B is curve A plus the computed stopping power due to excitation. Curve C adds to B the stopping power due to secondary electrons with kinetic energy greater than 300 Ry. Curve D is the Bethe formula with $I = 42.0$ eV. Circles are the ionization stopping-power measurements of Ref. 24, and triangles are the total stopping-power measurements of Ref. 25.

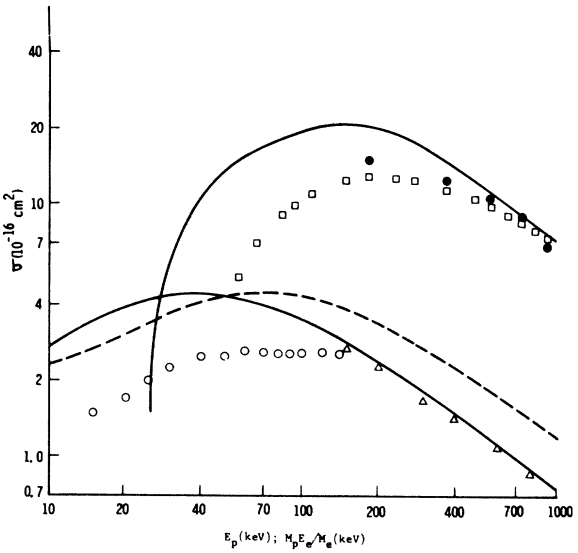

FIG. 7. Proton- and electron- (×10) ionization cross section of atomic nitrogen. Solid curves are our calculations, dashed curve is from Ref. 11; open circles, triangles, squares, and closed circles are from Refs. 20, 21, 26, and 23, respectively. The measured molecular cross sections are divided by 2.

power using the GOS calculated for $\epsilon \leq 200$ Ry. Solid curve B is the sum of the excitation and ionization stopping powers. Comparison of curve A with the results of Rudd and Jorgensen indicate that at 50 keV the calculated ionization stopping power is overestimated, and at 100 and 150 keV underestimated, relative to the measurements. This is merely a reflection of the disagreement seen in Fig. 5. The triangles are the measured total stopping-power results of Reynolds *et al.*[25] The sum of the computed excitation stopping power and the stopping power of Rudd and Jorgensen at 150 keV is within 2% of the measured total stopping power. However, at 50 and 100 keV the stopping power of Rudd and Jorgensen plus our computed excitation stopping power is significantly lower than the measured total stopping power, even though our excitation GOS are higher than the best calculations. The dashed curve D is the Bethe formula with $I = 42.0$ eV; curve C arises from choosing $E_B = 200$ Ry in Eq. (8). The difference between B and C is the contribution of the assumed δ function GOS for $\epsilon > 200$ Ry. The direct calculation does not agree with the Bethe formula until the incident proton energy is equal to or greater than 3 MeV. The results for protons on He indicate that, while the Bethe formula for stopping power breaks down at incident proton energies of 100 keV, the Born approximation with one-electron wave functions is not accurate to better than 25% at the same energy. The difficulty lies in the inability of this approach to accurately reproduce the measured $d\sigma/d\epsilon$ over a wide range of ϵ.

In Table III we list the computed total proton-ionization cross section and stopping power for He–Na, and in Table IV the total electron-ionization cross section. In Fig. 7 we show the computed proton- and electron-ionization cross sections for atomic nitrogen, Peach's proton calculation,[11] the results of Smith *et al.*[26] on electron ionization of atomic nitrogen and that of Rapp and Englander-Golden[23] for electrons on molecular nitrogen, and the results of deHeer *et al.*[20] and Hooper *et al.*[21] for protons on molecular nitrogen. The measured molecular cross sections have been divided by 2 to compare with the atomic calculations. The molecular cross sections are used for comparison because the atomic cross sections have been measured for incident electrons over a narrow energy range only. Where the atomic and half the molecular

TABLE II. Comparison of I/Z [eV/(nuclear charge)] with best estimates from Ref. 17.

Element	He	Li	Be	B	C	N	O	Fl	Ne	Na
I/Z(calc)	20.4	11.4	9.64	9.90	10.6	11.0	12.4	12.9	12.4	10.2
I/Z(expt)	21	13	16		13.5	12.6	12.6			

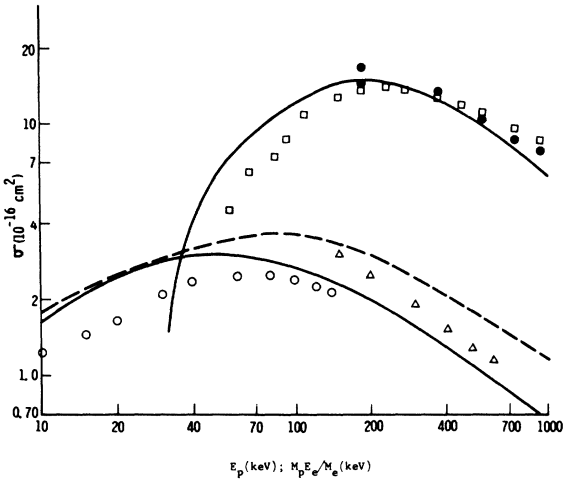

FIG. 8. Proton- and electron- (×10) ionization cross section of atomic oxygen. Solid curves are our calculations; dashed curve is from Ref. 11; the open circles, triangles, squares, and closed circles are from Refs. 20, 21, 27, and 23, respectively. The measured molecular cross sections are divided by 2.

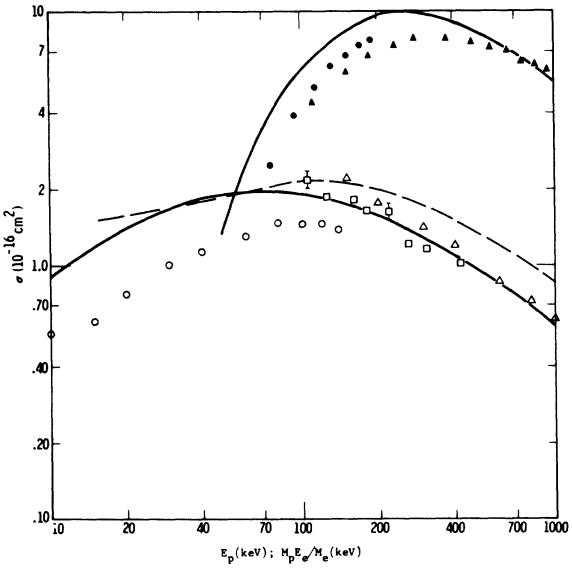

FIG. 9. Proton- and electron- (×10) ionization cross section of Ne. Solid curves are our calculations, dashed curve is from Ref. 11; the open circles, squares and triangles, and closed circles and triangles are from Refs. 20, 28, 21, 22, and 23, respectively.

measurements overlap in incident electron energy they are within experimental error. In addition, for clarity, here as in Figs. 8–10, the electron-ionization cross sections have been multiplied by 10. Our calculations are in good agreement (10%) with the measurements (which are in excellent agreement) for proton energy greater than 150 keV and electron energy greater than 300 eV. Peach's calculations here and in the heavier elements is a factor of 2 higher at energies where our calculations and experiment are in better than 20% agreement, showing the improvement attainable with the use of continuum orbitals more sophisticated than the hydrogenic ones. In Fig. 8 we show our proton- and electron-ionization cross sections for oxygen, Peach's proton calculation,[11] the electron-ionization measurements on atomic oxygen of Rothe *et al.*[27] and the molecular measurements of Rapp and Englander-Golden,[23] and the proton-ionization of molecular oxygen measurements of deHeer *et al.*[20]

TABLE III. Proton ionization and stopping-power calculations. First entry is the total ionization cross section in 10^{-16} cm^2, second entry is the stopping power due to ionization and excitation in 10^{-15} eV cm^2.

Atom/E(KeV)	10	20	40	70	100	200	400	700	1000
Li	11.5	8.63	5.16	3.24	2.40	1.25	0.75	0.46	0.34
	35.1	25.5	16.8	11.8	9.36	6.19	4.02	2.80	2.16
Be	9.17	8.76	6.10	4.01	3.00	1.66	0.91	0.56	0.41
	45.0	36.8	26.1	18.4	14.4	9.12	5.62	3.80	2.93
B	6.36	7.65	6.71	5.10	4.04	2.42	1.40	0.88	0.66
	31.1	29.5	24.6	19.7	16.2	10.5	6.69	4.50	3.48
C	4.06	5.78	5.71	4.77	3.99	2.57	1.54	1.00	0.75
	20.0	23.0	22.1	19.4	16.9	11.7	7.51	5.13	3.97
N	2.78	4.03	4.47	4.08	3.58	2.45	1.53	1.01	0.76
	14.6	17.4	18.6	17.8	16.4	12.3	8.37	5.98	4.58
O	1.70	2.55	3.04	2.98	2.72	1.99	1.30	0.87	0.66
	9.23	11.8	13.9	14.8	14.4	11.9	8.48	6.20	4.93
F	1.20	1.87	2.34	2.40	2.27	1.76	1.18	0.81	0.62
	6.26	9.10	11.5	13.0	13.2	11.8	8.86	6.75	5.54
Ne	0.87	1.39	1.81	1.96	1.90	1.54	1.07	0.74	0.58
	4.25	6.80	9.50	11.9	12.4	11.8	9.26	7.40	6.20
Na	14.6	9.81	5.81	3.83	2.99	1.89	1.16	0.76	0.57
	43.8	31.8	22.6	17.4	15.8	13.2	9.85	7.80	6.60

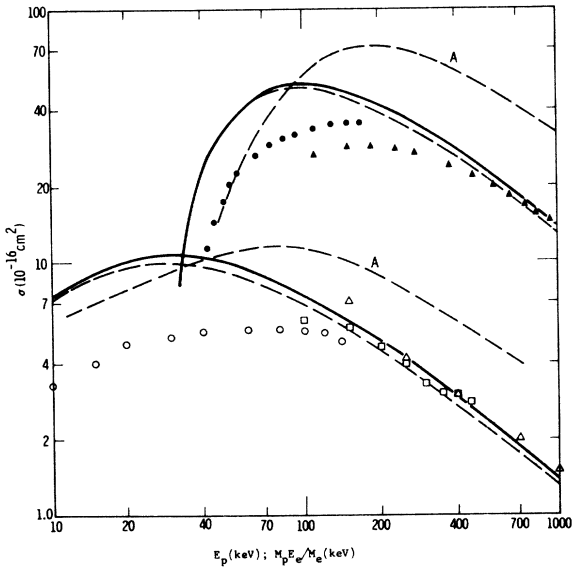

FIG. 10. Proton- and electron- (×10) ionization cross section of Ar. Dashed curves labeled A are from Ref. 11, unlabeled dashed curves are our $3p$ ionization calculations and solid curves are our $3p+3s$ ionization-cross-section calculations. Open circles, triangles, and squares, and the closed circles and triangles are from Refs. 20, 28, 21, 22, and 23, respectively.

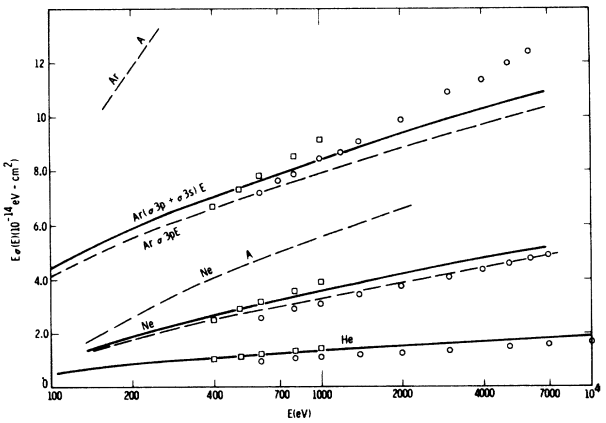

FIG. 11. $E_e\sigma(E)$ for electron ionization of He, Ne, and Ar. Dashed curves labeled A are for Ne $2p$ and Ar $3p$ from Ref. 11. Unlabeled dashed curves are our calculations for Ne $2p$ and Ar $3p$, with the solid curve the calculated total cross section. The open circles and squares are from Refs. 29 and 23, respectively.

and Hooper *et al.*[21] There is a 50% difference in the experimental proton-ionization cross section at 150 keV, with our calculation lying between the two sets of measurements. At 1 MeV our calculation is 15% smaller than the proton measurements, and at 540 eV the calculation is 20% below the electron-ionization data. In Fig. 9 we show our calculations for ionization of Ne by protons and electrons, Peach's proton calculation,[11] the electron-ionization measurements of Asundi and Kurepa,[22] and Rapp and Englander-Golden,[23] and the proton-ionization measurements of deHeer *et al.*,[20] Hooper *et al.*,[21] and Gilbody and Lee.[28] The measurements of deHeer *et al.* and Hooper *et al.* disagree as they do for oxygen, with the measurements of Gilbody and Lee lying between the two, as does our calculation. At 1 MeV the proton-ionization calculation differs from the measurement of Hooper *et al.* by 5%. From 300–550 eV the electron-ionization calculation is within 10% of the measurements of Rapp and Englander-Golden. In Fig. 10 we show our calculated cross sections for proton and electron ionization of the argon $3p$ and $3s$ shell, Peach's calculations,[11] and the data of Asundi and Kurepa,[22] Rapp and Englander-Golden,[23] deHeer *et al.*,[20] Hooper *et al.*,[21] and Gilbody and Lee.[28] As mentioned earlier, photoionization calculations indicate the calculated argon

TABLE IV. Computed electron total ionization cross section in 10^{-16} cm^2.

E(Ry)/Element	He	Li	Be	B	C	N	O	Fl	Ne	Na
0.40										
0.70		2.15	0.70							3.60
1.0		3.20	1.85	1.49	0.77	0.17				4.60
1.50		3.25	2.65	2.35	1.37	0.78	0.34	0.10	0.0026	4.20
2	0.054	2.90	2.65	2.80	1.90	1.17	0.62	0.30	0.18	3.65
4	0.404	1.95	2.10	2.85	2.50	1.91	1.22	0.85	0.58	2.10
7	0.510	1.28	1.45	2.28	2.20	2.04	1.47	1.18	0.91	1.50
10	0.480	1.00	1.13	1.85	1.90	1.85	1.47	1.25	0.99	1.31
20	0.335	0.58	0.65	1.12	1.23	1.20	1.02	0.92	0.83	0.85
40	0.210	0.32	0.36	0.640	0.722	0.728	0.632	0.582	0.55	0.41
70	0.138	0.195	0.23	0.398	0.458	0.470	0.415	0.384	0.37	0.34
100	0.103	0.142	0.165	0.292	0.339	0.354	0.313	0.296	0.281	0.26
200	0.058	0.078	0.089	0.160	0.188	0.200	0.178	0.169	0.165	0.148
500	0.026	0.034	0.039	0.071	0.085	0.091	0.084	0.079	0.078	0.067

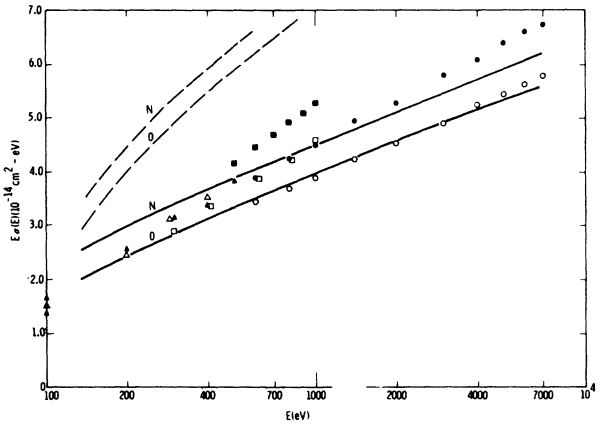

FIG. 12. $E_e\sigma(E)$ for electron ionization of atomic nitrogen and oxygen. Dashed curves are for $2p$ ionization from Ref. 11. Open triangles, squares, and circles are for nitrogen from Refs. 26, 23, and 29, respectively. Closed triangles, squares, and circles are for oxygen from Refs. 27, 23, and 29, respectively. All molecular cross sections are divided by 2.

$3p$ ionization GOS is in error at $K^2 = 0.0$. The calculations shown in Fig. 10 indicate that this error is not significant for the proton- and electron-ionization cross sections for the energy ranges considered.

Schram *et al.*[29] have measured electron-ionization cross sections in the 0.6–20-keV range. It is expected that in this range the cross section will approach an asymptotic limit, i.e., $\sigma(E_0) = A(\ln bE_0)/E_0$, where E_0 is the incident electron energy and A and b are constants characteristic of the target. In Fig. 11 we plot $E_0\sigma(E_0)$ versus $\ln E_0$ for He, Ne, and Ar and compare the results with the measurements of Schram *et al.*[29] and Rapp and Englander-Golden[23] (where the two sets of measurements overlap they differ by at least 20%). For He and Ne the calculations lie between and parallel to the measurements. Inokuti and Kim[30] have computed $E\sigma(E)$ for electrons on He by subtracting accurate discrete excitation cross sections from the total inelastic cross sections based on the Bethe sum rule. Between 500 and 7000 eV our calculated $E\sigma(E)$ differs from the expression of Inokuti and Kim by less than 3%. For Ne we show calculations for both $2p$ shell and total ionization. The $2s$ shell of Ne contributes about 10% to the total at high energy. At 6 keV the Ar calculation differs from the measurements by 10%. Thus, over a wide range of incident electron energies, the error in the Ar GOS, which leads to a factor of 2 error in the photo-ionization cross section, leads to no more than a 10% error in the electron-ionization cross section. Peach's Ne $2p$ and Ar $3p$ results are included.

In Fig. 12 we plot the calculated $E_0\sigma(E_0)$ versus $\ln E_0$ for atomic nitrogen (open points) and atomic oxygen (closed points) and the results of Schram *et al.*,[29] Smith *et al.*,[26] Rothe *et al.*,[27] and Rapp and Englander-Golden.[23] All molecular results are divided by 2. The calculations indicate the results for nitrogen should be higher than for oxygen. The experimental values show an opposite behavior. The results of Smith *et al.*[26] on atomic nitrogen and Rapp and Englander-Golden[23] on molecular nitrogen for 500–1000 eV agree with the calculations to 10%. The molecular nitrogen results of Schram *et al.* are 15% lower, but in good agreement with the calculated slope of $E_0\sigma(E_0)$ up to 7 keV. However for oxygen, all measurements are higher than the calculations, and while there is a significant disagreement between the slope of the measurements by Schram *et al.* and of those by Rapp and Englander-Golden, both are higher than the calculated value. Peach's results[11] are also plotted. Of course, this disagreement may be due to the comparison with molecular data for high-incident electron energy. At high-incident energies the cross section is dominated by the optical GOS and this is clearly

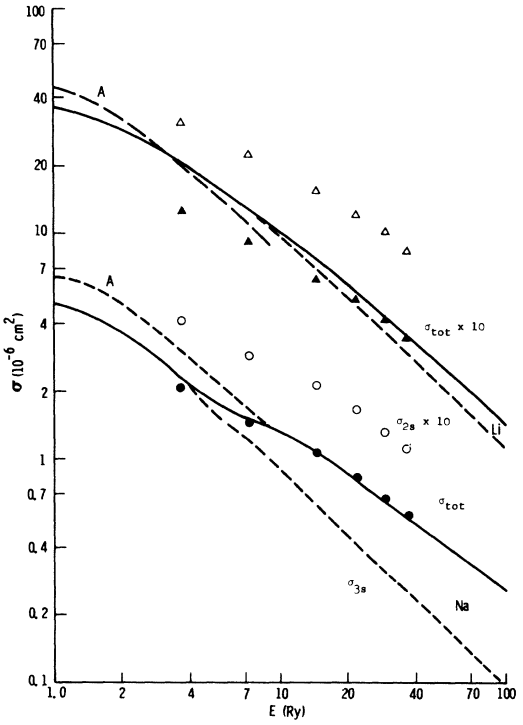

FIG. 13. Electron-ionization cross section of Li (×10) and Na. Dashed curves labeled A are from Ref. 11. Unlabeled dashed curves are our Li $2s$ and Na $3s$ cross-section calculations, and solid curves are our total cross-section calculations. Open circles and triangles are the measurements of Ref. 30 for Na and Li, respectively. Solid circles and triangles are the measurements fitted with our calculations at 500 eV.

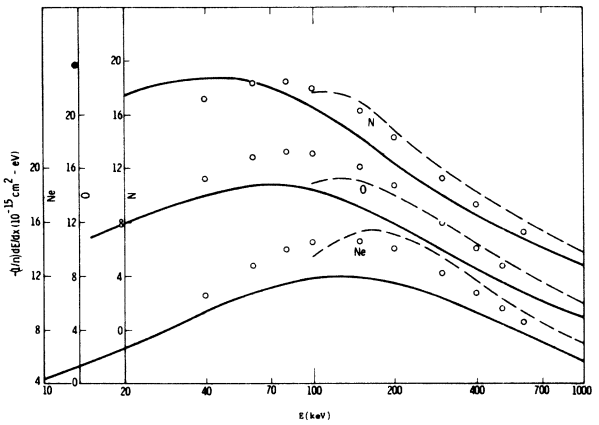

FIG. 14. Proton stopping power of Ne, O, and N. To each element corresponds a different ordinate. Solid curve is our direct calculation, dashed curve the Bethe formula with I taken from Table II, and open circles are from Ref. 25.

different for atoms and molecules. However, the measurements on atomic oxygen and nitrogen have not been carried to sufficiently high energy to show where the departure of the atomic from half the molecular cross section occurs. In Fig. 13 we compare our calculated Li 1s and 2s and Na 3s and 2p electron-ionization cross sections with Peach's calculations on Li 2s and Na 3s, and with the "absolute" measurements of McFarland and Kinney.[31] For convenience all the Li results are multiplied by 10. The absolute measurements depend on the assumption of 100% efficiency for a surface-ionization detector. The measurements are the open points. By fitting the data at 500 eV to our calculations we obtain the solid points. Assuming the calculations are correct then the surface-ionization efficiency is 0.5 for Na and 0.42 for Li.

Finally, in Fig. 14 we show the computed stopping power (the sum of excitation and ionization stopping power), the Bethe formula, using the computed mean excitation energies in Table II, and measurements of Reynolds *et al.*[25] The molecular measurements are divided by 2. The direct calculation underestimates, and the Bethe formula, with our computed mean excitation energy, overestimates the stopping power. Above 100 keV the direct calculation is no worse than 20% below the measured values. Again we attribute the error to the inability of the GOS to reproduce the correct $d\sigma/d\epsilon$ at large ϵ, though there are no measurements whereby this can be verified.

IV. NEUTRAL-NEUTRAL IONIZATION AND STRIPPING

The computation of atomic ionization GOS is time consuming even on the fastest computers currently available. However, once obtained, the GOS can be used in a wide variety of Born-approximation calculations. This would justify the large expense in computer time, were it not for the fact, as indicated by Levy's hydrogen calculations,[32] and by those of this section, that the Born approximation is, in general, a poor procedure for doing neutral-neutral ionization except at projectile energies greater than 1 MeV.

Born-approximation cross-section expressions for $A + B \rightarrow A' + B'$, where the primes indicate either or both A and B are elastically scattered, singly excited or singly ionized, are given by Bates.[33] In Fig. 15 we show calculated cross sections for ionization and stripping for a neutral He incident on He, Ne, and Ar. Stripping refers to ionization of the projectile and ionization to ionization of the target. For He + He the ionization and stripping cross sections are identical. For the elastic scattering factors we use the calculations of Lea.[34] In the computed He + He cross section in Fig. 15, the portion of the cross-section solid from 10–100 keV and dashed from 100–1000 keV, curve 1, includes only the processes where one He is excited or elastically scattered and the other is ionized. Elastic scattering plus ionization is at least a factor of 10 greater than excitation plus ionization over the range investigated. The solid curve from 100–1000 keV, curve 2, includes also the process He + He $\rightarrow$ He$^+$ + He$^+$. This mutual-ionization cross section peaks at 1 MeV. The calculation is in excellent agreement with the measurements of Wittkower *et al.*,[35] in poor agreement with the results of Puckett *et al.*,[36] and agrees roughly in shape with the swarm measurements of Barnett and Stier.[37] In Fig. 16 we show calculations for the partial stopping power in He + He collisions, and the measurements of Cuevas *et al.*[38] Partial stopping power is defined as the stopping power due to processes wherein the projectile suffers no change in charge. The curve labeled 1 includes only the process where the target is ionized and the projectile elastically scattered, curve 2 is curve 1 plus the process where either He atom is excited and the other elastically scattered, curve 3 is curve 2 plus the cross section for excitation of the projectile plus ionization of the target. Curve 4 is the measurements of Cuevas *et al.* At 400 keV the measurements are higher than the calculation, as one would expect from the distorted GOS. Near 100 keV the calculation and measurement are in good agreement.

The disagreement between the measurements of Wittkower *et al.*[35] and Puckett *et al.*[36] is attributed to the question of metastables in the He beam. That these calculations are in reasonable agreement with the stopping-power measurements and the cross-section measurements of Wittkower *et al.* should

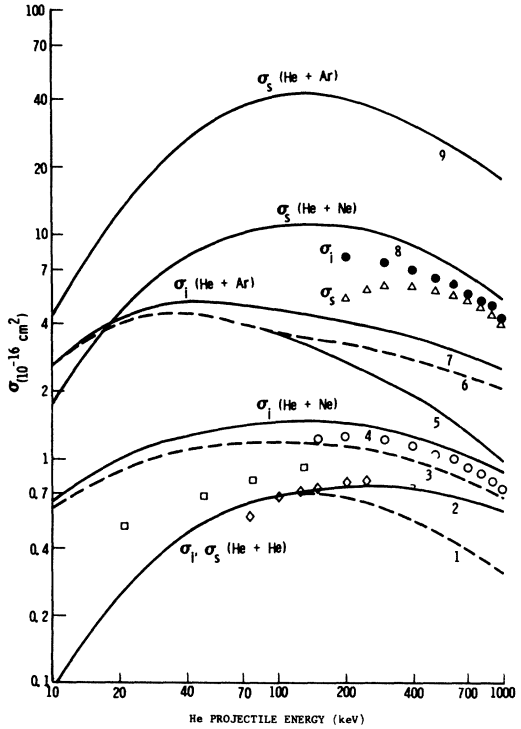

FIG. 15. Ionization and stripping cross sections for He projectile incident on He, Ne, and Ar. Curve 1 is the cross section for stripping or ionization of one He while the other is excited or elastically scattered. Curve 2 is curve 1 plus mutual ionization. Open diamonds, squares, and circles are for He + He ionization or stripping from Refs. 34, 36, and 35, respectively. Curves 8 and 9 are for stripping of the He projectile plus elastic scattering of Ne and Ar, respectively. Curves 3 and 4 are for ionization of Ne $2p$ and Ne $2p + 2s$, respectively, plus elastic scattering of the He projectile; curve 5 is for Ar $3p$ ionization plus He elastic scattering, curve 6 is curve 5 plus mutual ionization of He and Ar $3p$; and curve 7 is 6 plus Ar $3s$ ionization with He ionized and elastically scattered. Closed circles and open triangles are for ionization and stripping in He + Ar collisions from Ref. 35.

support the latter measurements. However, the agreement of calculation and measurement may be fortuitous. In the Born approximation for a projectile other than a proton the integral over momentum transfer is such that $(K^2_{\min})_{\text{proj}} \geq (K^2_{\min})_{\text{proton}} \times M_{\text{proj}}/M_{\text{proton}}$. Thus in integrating over K^2 and ϵ to determine the cross section for a 200-keV He projectile one includes only that region of the GOS over which one integrates for 50-keV protons (where the calculated ionization cross section is too high by a factor of 2).

Levy's calculations[32] indicate one can use the Born approximation to compute the hydrogen-ionization cross section in H + H and H + He collisions, and be in good agreement with experiment. We have shown that this, perhaps fortuitously, is also true in He + He collisions. However, as shown in Fig. 15, for stripping of He projectiles by Ne, curve 8, and Ar, curve 9, targets, the cross section goes as Z^2, where Z is the nuclear charge of the target. There are no data available for He + Ne, but Puckett *et al.*[36] have measured stripping for He + Ar, shown in Fig. 15. The calculation and experiment differ by at least a factor of 4. We also show the calculated ionization cross section for He projectiles on Ne, curve 4, and Ar, curve 7. For Ne we show the ionization cross section for He elastically scattered and Ne $2p$ ionized (dashed curve 3) and both $2s$ and $2p$ ionized. For proton ionization at 250 keV the cross section for ionization of the Ne $2s$ shell is less than 10% of the total cross section, while for an incident He projectile of 1 MeV the Ne $2s$ ionization cross section is 25% of the total. For Ar ionization we show the cross section for elastic scattering of He plus ionization of Ar $3p$, curve 5. Curve 6 is curve 5 plus the cross section for ionization of He and ionization of Ar $3p$. Curve 7 is curve 6 plus the cross section for Ar $3s$ ionized and He both elastically scattered and ionized. From 150 to 1000 keV the He + Ar ionization cross section is no more than a factor of 2 below the measurements of Puckett *et al.*, and the error may be due to metastables in the He beam.

V. CONCLUSIONS

We have attempted a broad survey of the applicability of the GOS (Born-approximation) approach to a wide variety of processes in atomic physics. In general, for protons of energy greater than 200 keV and electrons of energy greater than 300 eV the ionization calculations are in better than 20% agreement with experiment. For proton stopping power the results are less satisfactory (the cause of

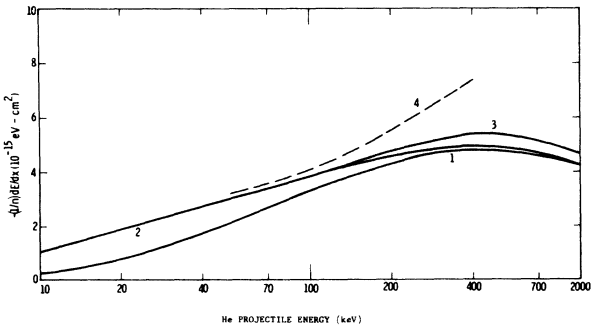

FIG. 16. Partial stopping power in He + He collisions. Curve 1 is for elastic scattering of the projectile plus ionization of the target. Curve 2 is 1 plus the stopping power due to either particle excited and the other elastically scattered. Curve 3 adds to 2 the stopping power due to excitation of the projectile plus ionization of the target. Curve 4 is the measurement from Ref. 37.

which is known), but one has agreement to 25% for incident proton energy greater than 200 keV. The ionization-cross-section differential in secondary electron energy (ϵ) can be wrong by a factor of 2 for some ranges of ϵ; and this is observed in calculations using ground-state wave functions more sophisticated than ours.[9] For neutral-neutral ionization collisions with projectile energy less than 1 MeV, it appears the Born approximation is poor except when both particles are light. We have done calculations for He + 2N collisions and compared the calculations with the measurements of Puckett *et al.* on $He + N_2$. The calculated stripping cross section is too high by a factor of 2, and the ionization cross section too low by a factor of 2 when compared to the measurements. If the measurements are correct, we can define light as $Z < 7$. At present we are studying reactions of the type $A^+ + B \rightarrow A^+ + B^+ + e$ and $A^{++} + B^+ + 2e$ with the GOS formalism to see if ion-neutral collisions are more accurately treated in the Born approximation than neutral-neutral collisions.

A recent study by Amusia *et al.*[39] on the cross-section differential in the incident-electron-scattering angle for keV electrons on the noble gases indicates that a one-electron approach using the central potential of Herman and Skillman leads to good agreement with experiment for Ne and Ar, but not for Kr and Xe. We are beginning a study of ionization-cross-section differential in both incident- and secondary-electron-scattering angles and secondary-electron energy to see if a one-electron approach is capable of reproducing experimental measurements of these more detailed cross sections.

ACKNOWLEDGMENT

The author wishes to thank Dr. Thomas A. Green of this laboratory for his valuable advice and critical reading of an earlier draft of this manuscript.

---

†Work supported by the U. S. Atomic Energy Commission.

[1]H. Bethe, Ann. Physik 5, 325 (1930).

[2]H. Bethe, *Handbüch der Physik* (Springer, Berlin, 1933), Vol. 24.

[3]S. M. Silverman and E. N. Lassettre, J. Chem. Phys. 40, 1265 (1964); E. N. Lassettre, M. E. Krasnow, and S. Silverman, *ibid.* 40, 1242 (1964).

[4]T. A. Green and J. M. Peek, Phys. Rev. 169, 37 (1968).

[5]A. R. P. Rau and U. Fano, Phys. Rev. 162, 68 (1967).

[6]Y.-K. Kim and M. Inokuti, Phys. Rev. 175, 176 (1968).

[7]W. J. B. Oldham, Jr., Phys. Rev. 174, 145 (1968).

[8]K. L. Bell, D. S. Kennedy, and A. E. Kingston, J. Phys. B 1, 204 (1968).

[9]K. L. Bell and A. E. Kingston, J. Phys. B 2, 653 (1969); 2, 1125 (1969).

[10]W. J. B. Oldham, Jr., Phys. Rev. 140, 1477 (1965).

[11]G. Peach, Proc. Phys. Soc. (London) 85, 709 (1965); 87, 375 (1966); J. Phys. B 1, 1088 (1968).

[12]F. Herman and S. Skillman, *Atomic Structure Calculations* (Prentice-Hall, Englewood Cliffs, N. J., 1963).

[13]E. J. McGuire, Phys. Rev. 175, 20 (1968).

[14]J. W. Cooper, Phys. Rev. 128, 681 (1962).

[15]E. J. McGuire, Sandia Research Report No. SC-RR-70-406 (unpublished).

[16]M. Inokuti and R. L. Platzman, in *Abstracts of Papers of the Fourth International Conference on the Physics of Electronic and Atomic Collisions* (Science Bookcrafters, Inc., Hastings-on-Hudson, N. Y., 1965).

[17]U. Fano, *Annual Review of Nuclear Science* (Annual Reviews Inc., Palo Alto, Calif., 1963), Vol. 13.

[18]I. V. Hertel and K. J. Ross, J. Phys. B 2, 285 (1969).

[19]R. A. Mapleton, Phys. Rev. 109, 1166 (1958).

[20]F. J. deHeer, J. Schutten, and H. Moustafa, Physica 32, 1766 (1966).

[21]J. W. Hooper, D. S. Harmer, D. W. Martin, and E. W. McDaniel, Phys. Rev. 125, 2000 (1963).

[22]R. K. Asundi and M. V. Kurepa, J. Electron. Control 15, 41 (1963).

[23]D. Rapp and P. Englander-Golden, J. Chem. Phys. 43, 1464, (1965).

[24]M. E. Rudd and T. Jorgensen, Jr., Phys. Rev. 131, 666 (1963).

[25]H. K. Reynolds, D. N. F. Dunbar, W. A. Wenzel, and W. Whaling, Phys. Rev. 92, 742 (1953).

[26]A. C. H. Smith, E. Chaplinger, R. H. Neynaber, E. W. Rothe, and S. M. Trujillo, Phys. Rev. 127, 1647 (1962).

[27]E. W. Rothe, L. L. Marine, R. H. Neynaber, and S. M. Trujillo, Phys. Rev. 125, 582 (1962).

[28]H. B. Gilbody and A. R. Lee, Proc. Roy. Soc. (London) A274, 365 (1963).

[29]B. L. Schram, F. J. deHeer, M. J. Van der Wiel, and J. Kistemaker, Physica 31, 94 (1965).

[30]M. Inokuti and Y. -K. Kim, in Ref. 16.

[31]R. H. McFarland and J. D. Kinney, Phys. Rev. 137, A1058 (1965).

[32]H. Levy II, in Ref. 16.

[33]D. R. Bates, *Atomic and Molecular Processes* (Academic, New York, 1962).

[34]J. D. Lea, Ph. D. thesis, University of Texas, 1963 (unpublished).

[35]A. B. Wittkower, G. Levy, and H. R. Gilbody, Proc. Phys. Soc. (London) 90, 581 (1967); 91, 862 (1967).

[36]L. J. Puckett, G. O. Taylor, and D. W. Martin, Phys. Rev. 178, 271 (1969).

[37]C. F. Barnett and P. M. Stier, Phys. Rev. 109, 385 (1958).

[38]J. Cuevas, P. Torres, and S. K. Allison, in Ref. 16.

[39]M. Ya. Amusia, N. A. Cherepkov, and S. I. Sheftel, Zh. Eksperim. i Teor. Fiz. 58, 618 (1970).